Research
Wastewater Treatment—Article

Electrochemical Removal of Chlorophenol Pollutants by Reactive Electrode Membranes: Scale-Up Strategy for Engineered Applications

Shuzhao Pei [a], Yi Wang [b], Shijie You [a,*], Zhanguo Li [b], Nanqi Ren [a]

[a] State Key Laboratory of Urban Water Resource and Environment, School of Environment, Harbin Institute of Technology, Harbin 150090, China
[b] State Key Laboratory of NBC Protection for Civilian, Beijing 102205, China

ABSTRACT

Chlorophenols (CPs) are significant refractory pollutants that are highly toxic to humans and other organisms. Reactive electrode membranes (REMs) show considerable potential in the electrochemical removal of refractory pollutants by allowing flow-through operations with convection-enhanced mass transfer. However, relevant studies are commonly performed on the laboratory scale, and there is no straightforward method that guarantees success in scaling up engineered REM reactors. In this study, we demonstrated that a tubular concentric electrode (TCE) configuration with a titanium suboxide ceramic anode and a stainless-steel cathode is suitable for large-scale CPs removal. Both theoretical and experimental results showed that the TCE configuration not only allows the electrode surface to be orthogonal to electric field lines everywhere, but also has an ohmic resistance that is inversely proportional to the length of the electrode. In addition, the TCE configuration can be operated in either the anode-to-cathode (AC) or the cathode-to-anode (CA) mode based on the flow direction, creating adjustable conditions for selective degradation of CPs. This was confirmed by 98% removal of 2,4-dichlorophenol (2,4-DCP) and 72.5% removal of chemical oxygen demand (COD) in the CA mode, in which the kinetic constant was one order of magnitude higher than that for the AC mode under flow-through single-pass operations. This can be explained by the lower activation energy and free energy in the CA mode, as revealed by theoretical calculations and experimental measurements. The TCE configuration is also suitable for a numbering-up strategy to scale up the electrochemical reactor without increasing the ohmic resistance or decreasing the specific electrode area, achieving 99.4% removal of 2,4-DCP with an energy consumption of 1.5 kW·h·m^{-3} when three TCE modules were employed. This study presents a suitable electrode design configuration for the REM reactor, offering effective strategies to bridge the "Valley of Death" encountered when scaling up the electrochemical removal of CP pollutants.

1. Introduction

Chlorophenols (CPs) are quantitatively significant pollutants released into the environment by chemical and pharmaceutical industry activities. They are also by-products of industrial processes in the manufacturing of polymers, dyes, textiles, resins, and explosives. CPs and their derivatives are mutagenic, carcinogenic, and immunogenic for humans and other organisms, and their treatment, disposal, and management have become serious challenges to stakeholders and health sectors. Most types of CPs are refractory to microbial degradation, making it imperative to develop more efficient methods for minimizing their pollution in water environments and ecological systems. Electrochemical oxidation has drawn increasing research interest for decentralized water decontamination because the application of electrons as traceless reactants offers several unique advantages, such as high efficiency, cleanliness, process integration, and ease of automation [1–3]. Electrochemical oxidation leads to the destruction of CP pollutants via direct electron transfer (DET) and indirect oxidation mediated by ·OH produced by water electrolysis.

Because low-concentration CPs can be oxidized faster than they can be transported to the anode surface, electrochemical oxidation of CPs is commonly controlled by diffusion. Reactive electrode membranes (REMs) offer a promising alternative for improving mass-transfer efficiency by flow-through electrolysis [4,5]. Compared with mechanical agitation and flow-by operations, REMs can conduct electrolysis in the flow-through mode with convection-enhanced mass transfer [6]. Thus, membrane electrodes show great promise for potential applications in water

* Corresponding author.
 E-mail address: sjyou@hit.edu.cn (S. You).

purification, such as pollutant removal, self-cleaning membrane, resource recovery, and seawater desalination [7–9].

Most studies on REMs are performed at the laboratory scale under well-controlled conditions. Consequently, a gap remains between experimental studies and practical applications. The process of scaling up a reactor from a lab prototype to an industrial plant is often referred to as the "Valley of Death," and there is no straightforward method that guarantees success in the scale-up of membrane electrodes. Unlike conventional chemical and biochemical reactors, where the geometric, kinematic, and thermal features are similar between the model and practical units, the electrode configuration of REMs is of prime importance [2,10,11]. Most flow-through electrochemical reactors are configured for plug-flow filtration [12,13] based on two parallel plate electrodes (PPEs) made of porous conductive materials, such as carbon nanotubes (CNTs) or Ti_4O_7 [14,15]. Although this mode provides a convenient and easy-to-handle platform to test the performance of electrode materials, challenges remain to scale up the electrochemical setup because increasing the electrode spacing or reactor volume increases the ohmic resistance and decreases the area-to-volume ratio. Hence, there is a compelling need to develop more efficient, reliable, and scalable electrode configurations to enable well-engineered industrial applications.

In principle, the appropriate electrode configuration should ① have a reasonable electric field distribution and low ohmic resistance, ② be effective for the removal of CP pollutants, and ③ allow modularization for easy-to-handle scale-up and engineering applications. Tubular electrodes with a cylindrical geometry are more favorable for increasing current density and power generation in energy conversion systems, such as solid oxide fuel cells (SOFCs), polymer electrolyte membrane fuel cells (PEMFCs), and vanadium redox flow batteries (VRFBs) [13,16–18]. Inspired by these successful applications, we attempted to bridge the "Valley of Death" for scaling up REMs by developing a tubular concentric electrode (TCE) configuration for the engineered application of electrochemical CPs removal.

In this study, we developed a TCE configuration containing an inner titanium suboxide (TiSO) tube (ceramic membrane anode) and outer stainless-steel (SS) tube (cathode), which allows the wastewater stream to flow through the two tubes in either the anode-to-cathode (AC) or cathode-to-anode (CA) direction. The tubular TiSO was selected as the anode material because its conductivity approaches that of metals, and its corrosion resistance is close to that of ceramics. The unique advantages of high conductivity, good stability, high oxygen evolution potential, and low cost make it a promising anode material for water purification [19]. First, we investigated the electric field distribution for different electrode configurations using software simulation and electrochemical validation. Second, we tested the electrochemical removal of typical biorefractory CP pollutants (i.e., 2,4-dichlorophenol (2,4-DCP)) under AC and CA flow modes, and the relevant mechanisms were elucidated using theoretical calculations and experimental data. Finally, we proposed a numbering-up strategy for scaling up the TCE module and flow-through reactor and tested its suitability for engineered water decontamination in single-pass mode. The primary objective of this study was to determine a reasonable electrode configuration for the scale-up of the REM reactor for CP pollutants removal.

2. Materials and methods

2.1. Materials

All purchased reagents were of analytical grade if there is no special statement and used without further purification. Sodium perchlorate ($NaClO_4$), 2,4-DCP, and chromatographic-grade methanol were purchased from Sinopharm Chemical Reagent Co., Ltd. (China), and the solution was prepared using ultrapure water obtained from a Milli-Q system (18.2 MΩ·cm at (22 ± 1) °C). The TiSO electrode was designed and manufactured according to the procedures described in our previous study [19].

2.2. Experimental setup and operation

The electrolysis experiments were conducted in a Plexiglas cylindrical electrolytic cell with a total volume of 3.8 L (220 mm × φ 150 mm) at room temperature ((25 ± 1) °C). The cell contained a tubular TiSO anode (outer diameter, 30 mm; thickness, 3 mm; length, 143 mm; projected area, 132.9 cm²) and a SS cathode (140 cm²). The electrodes were connected to a direct current (DC) power supply by copper wires. Prior to the tests, the TiSO electrodes were cleaned for 10 min in a 0.5 mol·L⁻¹ $NaClO_4$ solution at a current density of 30 mA·cm⁻². The initial influent contained 0.1 mol·L⁻¹ $NaClO_4$ and 10 mg·L⁻¹ 2,4-DCP at a neutral pH (7.2 ± 0.2), and the electrolytic cell was operated in single-pass mode without recirculation. The experiments were performed with 10 min of stabilization without the application of current, and 5 mL aliquots were withdrawn from the effluent at specified intervals, followed by immediate filtration with cellulose acetate filters (0.22 μm) before chemical analysis.

The hydraulic retention time (HRT, s) of the system was calculated by

$$HRT = \frac{d}{J} = \frac{dA}{Q} \tag{1}$$

where J (m·s⁻¹) is the permeation flux, d (m) is the thickness of a single TiSO anode, A (m²) is the anode area, and Q (m³·s⁻¹) is the flow rate.

2.3. Electrochemical characterization

Electrochemical characterization was performed with a SS counter electrode and Ag/AgCl (saturated KCl aqueous solution (KCl_{aq}), 0.198 V vs standard hydrogen electrode (SHE)) reference electrode. Cyclic voltammetry (CV) was performed at a sweep rate of 100 mV·s⁻¹ in a three-electrode cell in the 2,4-DCP degradation phase. Electrochemical impedance spectroscopy (EIS) was conducted between 10 mHz and 100 kHz using a sinusoidal potential perturbation with an amplitude of 5 mV.

2.4. Analyses

The 2,4-DCP concentration was determined using a ultrahigh-performance liquid chromatography (UPLC) instrument (Agilent 1200, USA) equipped with a photodiode array detector (PDA) and a reversed-phase C18 column (50 mm × φ 2.1 mm, Waters, USA). The mobile phase consisted of water/methanol (30:70, v/v) at a flow rate of 0.1 mL·min⁻¹. The degraded intermediates of 2,4-DCP were analyzed qualitatively based on the mass-to-charge ratio using UPLC with electrospray ionization mass spectrometry (UPLC–ESI/MS) (Agilent 6460, USA) with mobile phase A (ultrapure water) and B (chromatographic-grade acetonitrile). High-resolution mass spectra were collected for range of the mass-to-charge ratio (m/z) 80–220 using negative continuum mode with a scanning time of 0.15 s, and the suspected intermediates were fragmented in the collision cell. The ionization source was set up with a capillary voltage of 3 kV, temperature of 200 °C, and desolvation temperature of 550 °C. The samples (20 μL) were analyzed in duplicate to ensure the accuracy and repeatability of the mass spectroscopy measurements. Chemical oxygen demand (COD)

was determined using an LH-3BA spectrophotometer (Lianhua Technology Co., Ltd. (China), chemical reagent type number: LH-D/E).

Energy consumption normalized per order (E_{EO}) of contaminant was calculated by Ref. [20]:

$$E_{EO} = \frac{UjA}{Q\log\left(\frac{C_f}{C_p}\right)} \times 10^{-3} = \frac{UI}{Q\log\left(\frac{C_f}{C_p}\right)} \times 10^{-3} \tag{2}$$

where E_{EO} (kW·h·m^{-3}) is the volumetric energy consumption required to reduce the organic contaminants by one order, U (V) is the average cell voltage; j (mA·cm^{-2}) is the current density, I (A) is the current, and C_f (mg·L^{-1}) and C_p (mg·L^{-1}) are the feed and permeate concentrations, respectively.

The current efficiency for oxidation was calculated by

$$CE(\%) = \frac{(COD_f - COD_p)bFV}{M_{O_2}It} \times 10^{-3} \times 100\% \tag{3}$$

where COD_f (mg·L^{-1}) and COD_p (mg·L^{-1}) are the COD concentrations of the feed and permeate, respectively, b (4) is the stoichiometric coefficient for number of electron transfer, F is the Faraday constant (96 485 C·mol^{-1}), V (L) is the volume treated over duration t, and M_{O_2} is the equivalent molar mass of oxygen (32 g·mol^{-1}).

2.5. Electric field simulation

Simulations were conducted on the PPE, tubular/planar electrode (TPE), and TCE configurations using COMSOL Multiphysics software (version 5.5; Palo Alto, USA). The models were used to simulate the electric field distribution for different electrode configurations using the definition of electric field strength:

$$E = -\nabla\varphi \tag{4}$$

where E is the electric field strength, and φ is the electric potential.

2.6. Theoretical calculations

Density functional theory (DFT) calculations were conducted using Gaussian software. The activation energy (E_a, kJ·mol^{-1}) for DET oxidation as a function of electrode potential was calculated according to Marcus theory. The calculation for the DET reduction reaction is similar and not shown.

$$E_a = \frac{\lambda_f}{4}\left[1 - \frac{96.5\left(E - E^0\right)}{\lambda_f}\right]^2 \tag{5}$$

where λ_f (kJ·mol^{-1}), which reflects the total reorganization energy for the electron-transfer oxidation reaction, can be calculated by subtracting ΔG^0 (kJ·mol^{-1}) of the reactant from that of the product with the same geometry. E (V) is the electrode potential vs SHE, and E^0 (V) is the standard potential of the DET reaction of the reactant, which can be determined thermodynamically as

$$E^0 = -\frac{\Delta_r G^0}{nF} - E_{abs}^0 \tag{6}$$

where $\Delta_r G^0$ (kJ mol^{-1}), which represents the free energy of reactant oxidation, can be calculated using the ΔG^0 determined from the optimized geometric structure of the reactant and product. n ($n = 1$) is the number of transferred electrons, and E_{abs}^0 is the reference absolute standard potential of the SHE (4.28 eV). The calculations were performed according to procedures described in previous studies [6,21].

3. Results and discussion

3.1. Electric field distributions of different electrode configurations

The spatial distribution of the electric field significantly affects electrochemical reactions because it is closely linked to charged ion transport [13,22–25]. In other words, electrochemical reactions only occur in the region of the electrode surface where the electric field lines reach, and vice versa. Because the electric field distribution is closely related to the electrode configuration, we used COMSOL modeling to visualize and quantitatively analyze the electrostatic field of three typical electrode configurations for wastewater treatment [13]: PPE, TPE, and TCE. As shown in Fig. 1, the symmetric PPE and TCE configurations exhibited the most uniform electric field distributions, whereas an asymmetric electric field was observed for the TPE configuration, which is similar to the results found by Hankin et al. [23] in a photoelectrochemical reactor and Sun et al. [26] in an electrochemical reactor [26]. This clearly suggests that complete utilization of the anode area could be achieved with the PPE and TPE configurations. However, less than 1/3 of the area of the tubular anode was active for the TPE configuration because the equipotential lines are always perpendicular to the electric field at each of their crossings. The electric field points away from the anode plane and toward the cathode plane. Because the charges are equal and opposite, the electric fields sum in the interpolar region, whereas they cancel each other out to zero in the region outside of the two electrodes [26]. In other words, only the electrode surfaces normal to each other are electrochemically active, and no transformation occurs in other regions. This can be easily visualized experimentally by observing the electrodeposition of a Cu film on only the front side of an SS disc (Fig. S1 in Appendix A). Note that the small amount of Cu film deposited at the edges of the back side was caused by the molecular diffusion of Cu^{2+} under a concentration gradient.

For the same anode, the cathode geometry can have a significant impact on the electric field distribution. Clearly, a uniform interelectrode electric field distribution is essential to effectively utilize the electrochemically active area because the ions can diffuse along the field lines, which has been proven to be efficient for water disinfection [24]. These results suggest that when
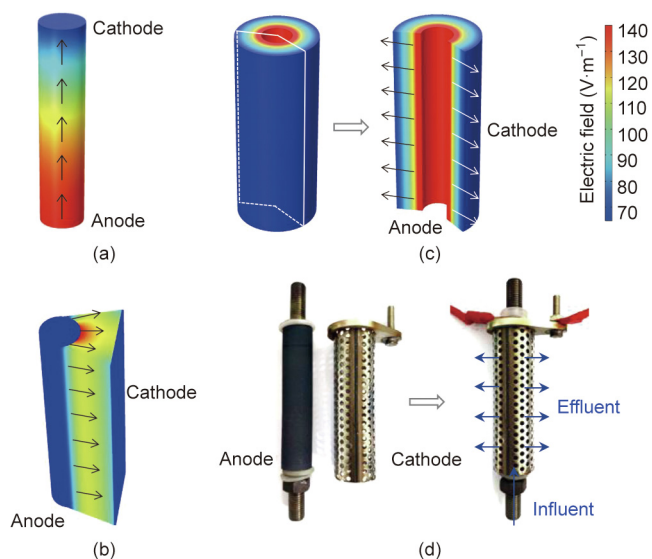

Fig. 1. COMSOL simulations of the electrostatic field for the (a) PPE, (b) TPE, and (c) TCE configurations with front and sectional views; (d) optical image of the TCE module.

designing a flow-through electrolytic cell, the surface of the electrode should be orthogonal to the electric field lines everywhere to maximize the effective electrochemically active area of the electrode. In accordance with this principle, the PPE design is more suitable for plug-flow electrolysis, whereas the TCE design is more rational for encompassed-flow electrolysis.

3.2. Dependence of ohmic resistance on electrode configuration

When the anode is polarized by passing current through the electrolytic cell, the voltage drop U (V) is determined by the equilibrium potential difference and overpotential [27]:

$$U = U_{min} + \eta_A + \eta_D + \eta_{ohm} \tag{7}$$

where U_{min} (V) is the theoretical minimum voltage required for electrolysis, η_A (V) is the activation overpotential dependent on a suitable catalyst, η_D (V) is the diffusion overpotential due to concentration polarization, and η_{ohm} (V) is the ohmic overpotential caused by the electrode material, configuration, and electrolyte [27]. For a given electrolytic system under flow-through operation, η_{ohm} is the dominant contributor to the cell voltage and thus energy consumption under constant-current electrolysis. Herein, the ohmic overpotential is calculated according to Ohm's law:

$$\eta_{ohm} = I\Sigma R_{ohm} \tag{8}$$

where ΣR_{ohm} (Ω) is the sum of the ohmic resistances.

It is worth noting that the electrode configuration may have a significant impact on the magnitude of the ohmic resistance. For example, based on an identical anode diameter (29 mm), axial length (142 mm), and electrolyte (0.1 mol·L^{-1} NaClO$_4$, pH 6.5), the ΣR_{ohm} value of the TCE configuration (2.1 Ω) was 89.3% and 83.3% lower than those of the PPE (19.8 Ω) and TPE (12.6 Ω) configurations, respectively, according to the x-intercept in the Nyquist plot of the EIS data (Fig. 2(a)). This difference could result from the difference in ion transport in the electrolyte in the interpolar space for the two systems. For the PPE configuration, the ohmic resistance is positively proportional to the axial length of the reactor, as follows:

$$R_{ohm}^{PPE} = \frac{L}{\kappa A} = \frac{L}{\kappa \pi r^2} \rightarrow R_{ohm}^{PPE} \propto L \tag{9}$$

where κ (S·m^{-1}) is the specific conductivity of the interpolar electrolyte, L (m) is the axial length of the tubular reactor, A (m^2) is the electrode area, and r (m) is the electrode radius. According to Eq. (9), R_{ohm}^{PPE} is a function of L, κ, and r. Therefore, if κ and r are known constants, R_{ohm}^{PPE} is only a function of L. That is, the ohmic resistance of the PPE configuration is considerably more sensitive to the scale of the reactor, and scaling up the electrolytic cell by increasing the axial length of the tubular reactor will lead to a linear increase in the ohmic resistance. In contrast, when r_1 and r_2 are fixed, the ohmic resistance of the TCE configuration is inversely proportional to L, suggesting that increasing the axial length of the cell adds value by lowering the ohmic loss (Eq. (10)) and energy consumption (Eq. (2)), rather than the inverse.

$$R_{ohm}^{TCE} = \frac{\ln(r_2/r_1)}{2\kappa\pi L} \rightarrow R_{ohm}^{TCE} \propto L^{-1} \tag{10}$$

where r_1 is the radius of the tubular anode, and r_2 is the radius of the tubular cathode.

Despite minor differences in ΣR_{ohm} values between the PPE and TCE configurations in small lab-scale prototype cells, scaling up these two configurations would lead to opposite behaviors of their ΣR_{ohm} values with increasing reactor volume (Figs. 2(b) and (c)). The decreased ohmic resistance of the TCE system becomes more significant when the conductivity of the solution is low (e.g.,
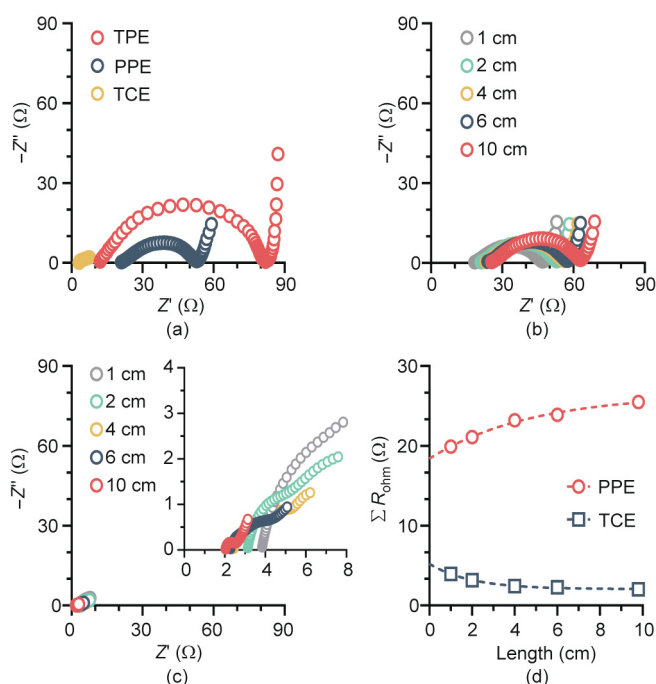

Fig. 2. EIS spectra for (a) different electrode configurations and (b) PPE and (c) TCE tubular reactors with various axial lengths; (d) total internal resistance (ΣR_{ohm}) as function of TCE length.

domestic sewage and groundwater) [28]. As shown in Fig. 2(d), the calculated ΣR_{ohm} value of the PPE configuration was 16 times that of the TCE configuration when the axial length of the tubular reactor was increased from 1 to 14 cm (Eqs. (9) and (10)). The TCE configuration was compact with a small electrode spacing and large electroactive area, considerably enhancing electron transfer and lowering the internal resistance [29].

Together, the combination of experimental results and theoretical verification demonstrate that the TCE configuration is more favorable for scaling up REMs owing to its uniform electric field and low ohmic resistance. Similarly, Lei et al. [30] reported efficient phosphate recovery (> 50 %) using a scalable prototype with a tubular SS cathode in a columnar electrochemical reactor over 173 days. The unique advantages of the amplified TCE configuration enabled the application of a scaled-up membrane electrode system [31]. Next, we shifted our focus to the engineered application potential of the TCE system for wastewater treatment.

3.3. Electrochemical removal of 2,4-DCP by the REM module

The electric field between the anode and cathode in the TCE configuration exhibited a uniform distribution, suggesting that efficient faradaic reactions occurred. The stream flow sequence, upstream from the anode to the cathode (AC mode) or downstream from the cathode to the anode (CA mode), has a crucial impact on the electrochemical reactions. Thus, we examined a tubular concentric TiSO anode/SS cathode REM reactor for the electrochemical removal of 2,4-DCP (10 mg·L^{-1}) with a NaClO$_4$ (0.1 mol·L^{-1}, pH 6.5) electrolyte under flow-through operation with different flow directions, current densities, and flow rates. Electrocatalytic reduction of 2,4-DCP occurs by accepting electrons at the cathode, whereas oxidation reactions occur at the TiSO anode. The anodic oxidation and cathodic reduction are coupled by the hydraulic connection of the flow stream between the electrodes.

A series of experiments were conducted to investigate the removal of 2,4-DCP at a current density of 5 to 30 mA·cm^{-2} and a flow rate of 15 to 120 mL·min^{-1}. As shown in Fig. 3(a), increasing the current density from 5 to 30 mA·cm^{-2} increased 2,4-DCP removal from 5%–28% to 18%–71% in AC mode. Because the limiting current density (0.6 mA·cm^{-2}) for the anodic oxidation of 10 mg·L^{-1} 2,4-DCP was considerably lower than the applied current density, 2,4-DCP was degraded under diffusion-controlled conditions. Nevertheless, when the flow velocity was increased in the range 15–120 mL·min^{-1}, the mass transfer coefficient increased from 2.5×10^{-6} to 2×10^{-5} m·s^{-1}. The decrease in retention time from 160 to 20 s under continuous operation resulted in a 70.7%–78.5% decrease in 2,4-DCP removal under AC mode. Similar results were also reported by Wang et al. [32], who found enhanced electrochemical oxidation efficiency at lower flow rates and higher applied current densities. Similarly, for CA mode, 2,4-DCP removal increased from 30%–85% (5 mA·cm^{-2}) to 81%–99% (30 mA·cm^{-2}) with increasing current density and decreased from 85%–99% (15 mL·min^{-1}) to 30%–81% (120 mL·min^{-1}) with increasing flow rate. The rate constant obtained under CA mode was one order of magnitude greater than that under AC mode (Figs. 3(c) and (d)), indicating the inherent dependence of synergistic cathode/anode interactions on the flow direction. Fig. S2 in Appendix A compares 2,4-DCP removal under the two operational modes at 20 mA·cm^{-2} and 60 mL·min^{-1}. Under CA mode, almost complete removal of 2,4-DCP was achieved after 5 min of electrolysis, compared with only 16.8% removal under AC mode. Based on a flow rate of 60 mL·min^{-1}, raising the current density from 5 to 30 mA·cm^{-2} increased the rate constant from 0.19 to 0.21 min^{-1} in CA mode, which is approximately 11.2–78.1 times that in AC mode (Fig. 3(c)). When the current density was fixed at 20 mA·cm^{-2}, increasing the flow rate from 15 to 120 mL·min^{-1} enhanced the oxidation rate because of improved flow-through convective diffusion in the porous structure of the anode. This accounts for the increase in the rate constant from 0.13 to 0.28 min^{-1} in CA mode, which is approximately 6.7–11.2 times that in AC mode (Fig. 3(d)). The kinetic behavior of 2,4-DCP oxidation in CA mode appeared to be more sensitive to the flow rate, as indicated by the nearly one order of magnitude higher area-normalized apparent rate constant (0.036–0.079 m·s^{-1}) compared to that for AC mode (Table S1 in Appendix A). This implies that ·OH-mediated oxidation was predominantly limited by mass transfer following cathodic activation (discussed below) when the wastewater stream flowed from the cathode to the anode.

In addition, water electrolysis resulted in the release of H$^+$ near the anode and OH$^-$ near the cathode, and the difference between CA and AC modes was also associated with differences in the migration of H$^+$ or OH$^-$, particularly at high current densities. In CA mode, OH$^-$ produced from the cathodic hydrogen evolution reaction (HER) diffused to the anode, resulting in a slight increase in the pH value near the anode due to neutralization of protons produced from water oxidation (Fig. S3 in Appendix A). In this case, deprotonated 2,4-DCP (pK_a = 7.8) was more likely to be adsorbed on the anode via electrostatic interactions, which facilitated the subsequent anodic oxidation. As shown in Fig. S4 in Appendix A, the CV curve exhibited a minimum potential of 1.66 V vs SHE for 2,4-DCP oxidation, and the intensity of the oxidative peaks was sensitive and positively related to the pH value. This indicates that 2,4-DCP oxidation is more favorable under higher pH conditions. Similarly, the typical oxidative intermediates, such as 2-CP and 4-CP, had pK_a values of 8 to 9 [33], making them more reactive at higher pH values. Together, these factors allowed the TCE reactor to degrade 2,4-DCP with a maximum overall COD removal of 72.5% (Fig. 3(e)) and a current efficiency of 35.5% (Fig. 3(f)) under CA operation, which are considerably higher than the values under AC operation.

3.4. Mechanistic insight into the impact of hydraulic flow

To further elucidate the 2,4-DCP degradation mechanism of the TiSO-based TCE reactor, the intermediate products were analyzed using UPLC–quadrupole–time-of-flight (UPLC–Q–TOF) mass spectrometry based on the mass-to-charge ratio (m/z). For AC mode, the results (Fig. S5 in Appendix A) matched those reported in previous studies, where six types of typical intermediates were detected during the electrochemical oxidation of 2,4-DCP [34,35]. In contrast, different intermediate products were detected for CA mode, indicating the reaction pathway and selectivity depend on the reaction sequence determined by the flow direction. Fig. S6 in Appendix A shows the accumulation of chlorinated dihydroxybenzenes (2 or 3) (m/z = 142.9342) and chlorinated benzoquinones (4 or 5) (m/z = 140.9376), which were characterized as the main intermediates in AC mode (Fig. 4). The reactions involve direct and indirect anodic oxidation of 2,4-DCP and direct cathodic reduction of chlorinated benzoquinone. In comparison, the characteristic intermediates observed for CA mode were phenol (m/z = 93.1581) and CPs (8 or 9) (m/z = 126.7408), whose relative abundance increased within the first 2 min, followed by a rapid decline without noticeable accumulation. Therefore, the cathodic reduction of
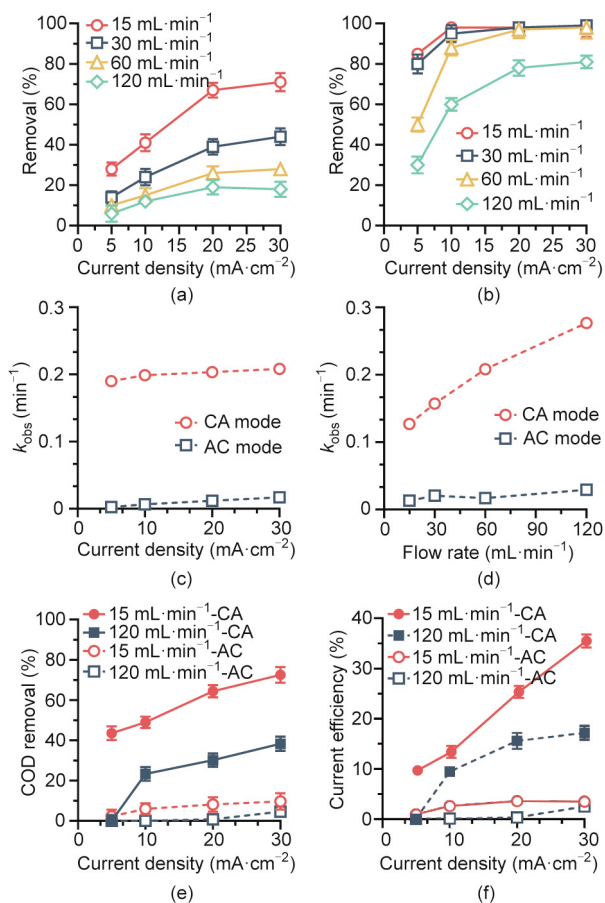

Fig. 3. 2,4-DCP removal performance of the TCE reactor as a function of flow direction, current density, and flow rate. Removal efficiency in (a) AC and (b) CA modes as a function of current density and flow rate. Removal kinetics as a function of (c) current density at a flow rate of 60 mL·min^{-1} and (d) flow rate at a current density of 20 mA·cm^{-2} for both flow modes (K_{obs} is the observed rate constant). (e) COD removal and (f) current efficiency in AC mode (hollow symbols) and CA mode (solid symbols) as a function of current density and flow rate (AC: waterstream from anode to cathode; CA: waterstream from cathode to anode). Influent solution ([2,4-DCP] = 10 mg·L^{-1}, [NaClO$_4$] = 100 mmol·L^{-1}) was electrolyzed.

2,4-DCP and the anodic oxidation of phenol (10), hydroquinone (11), or catechol (12) are the most probable relevant reactions.

The mechanistic insight into the impact of the flow mode can also be explained in the context of the difference in free energy for the two operational modes predicted by DFT calculations (Fig. 4). As shown in Fig. S7 in Appendix A, the activation energy for electro-reduction was lower than that for electro-oxidation. Specifically, the minimum potentials required for anodic oxidation of 2,4-DCP, phenol (10), hydroquinone (11), and catechol (12) were 1.90, 1.85, 1.40, and 1.50 V vs SHE, respectively, whereas the cathodic reduction of CPs (8 or 9), chlorinated benzoquinones (4 or 5) occurred at maximum potentials of −1.55, −1.55, −0.55, and −0.75 V vs SHE, respectively. Considering the similar redox nature of the DET of dihydroxybenzenes (11 or 12) and benzoquinones (6 or 7), the calculation of the overall free energy was simplified based on 1,4-benzoquinone (7). As revealed in Table S2 in Appendix A, the free energy was calculated to be −488.4 and −684.7 kJ·mol^{-1} for AC and CA modes, respectively, at anode and cathode potentials of 2.38 and −1.45 V vs SHE, respectively, indicating a more thermodynamically favorable pathway for 2,4-DCP degradation under CA mode. As shown in Fig. 4(c), the conversion of *o*-chloro-dihydroxybenzene (3) to *o*-chloro-*p*-benzoquinone (5) was the limiting step for AC mode, which could be alleviated by implementing cathodic reduction before anodic oxidation. Owing to the considerably lower energy required for the dechlorination of CPs (8 or 9) (−250.4 kJ·mol^{-1}), cathodic reduction allows the more thermodynamically feasible dechlorination process to occur under a low applied cathode potential ($E^0 = -1.15$ V vs SHE). The formation of phenol as a key intermediate increases the activity for subsequent anodic DET oxidation (Fig. S7) and ·OH attacks, which provides the most likely explanation for the high activity and high selectivity. Compared with that in AC mode, a high electric energy input is not required because cathodic reduction greatly decreases the minimum potential and activation energy (U_{min} in Eq. (7)) of 2,4-DCP, resulting in enhanced current efficiency and electrochemical mineralization (Fig. 3). Another advantage of CA operation is the lower biotoxicity of the dechlorinated intermediates (Fig. S8 in Appendix A). In this way, we were able to effectively destroy more CP pollutants with the removal efficiency more than 85% (Fig. S9 in Appendix A; 20 mA·cm^{-2} and 60 mL·min^{-1}).

3.5. Numbering-up strategy for scaling up the REM module

Based on the above results, we attempted to scale up the flow-through electrolytic reactor based on the TCE configuration. In an electrochemical system, the area-to-volume ratio (A/V), that is, the specific electrode area (A_S), is the key parameter that determines the inherent conversion capacity of the electrochemical system [36]. The importance of A_S must be emphasized when the REM is scaled up to a larger size.

If the electrochemical system is scaled up along the axial length of the tubular reactor (PPE), the size and volume of the reactor will increase at the expense of a decline in A_S:

$$A_S^{PPE} = \frac{A}{V_{liquid}} = \frac{\pi r^2}{\pi r^2 L} = \frac{1}{L} \rightarrow A_S^{PPE} \propto L^{-1} \quad (11)$$

where L is the axial length of the electrolytic cell, and r is the radius of the planar electrode. Although it is theoretically possible to scale up a PPE reactor by increasing the electrode area, this not only adds complexity to electrode fabrication and process integration but also causes nonuniformity in the primary current distribution on the electrode [37].

Because the TCE configuration allows water to flow through the side wall of the anode, the cylindrical geometry provides a higher surface-to-volume ratio than that of the planar geometry. Scaling up the electrolytic cell can be achieved simply by numbering up the TCE arrays, in which A_S is independent of the axial length and volume of the reactor:

$$A_S^{TCE} = \frac{nA}{V_{liquid}} = \frac{2\pi r_1 nL}{\pi (R^2 - nr_1^2) L} = \frac{2nr_1}{R^2 - nr_1^2} \quad (12)$$

where r_1 is the radius of the inner tube of a single TCE module, R is the radius of the reactor, and n is the number of TCE modules. This design enables modularization of TCE arrays with arbitrary axial lengths and numbers to create integrated electrolytic reactors that depend on the amount of wastewater to be treated in engineered applications.

To evaluate the effectiveness of the numbering-up strategy, we designed an electrochemical reactor containing TiSO TCE arrays with n = 1, 2, and 3 (Fig. 5(a)) and tested the overall performance
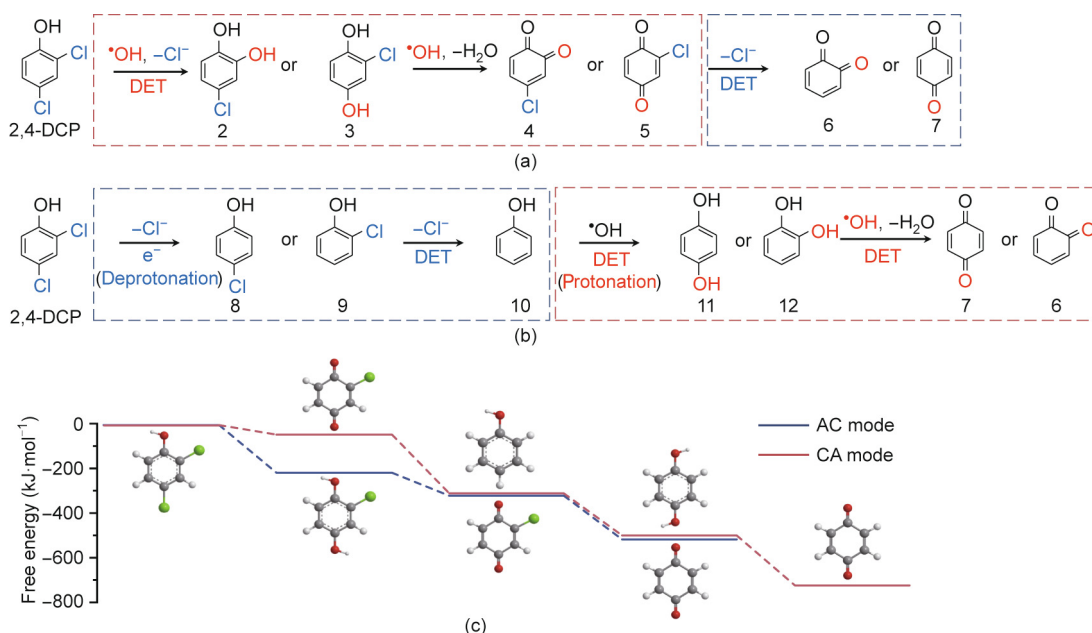

Fig. 4. Mechanism under (a) AC and (b) CA mode, and (c) DFT calculation for 2,4-DCP degradation at anode and cathode potentials of 2.38 and −1.45 V vs SHE, respectively.

of 2,4-DCP degradation (10 mg·L^{-1}). Increasing the n value resulted in a higher removal efficiency, higher current efficiency, and lower energy consumption due to the increased area-to-volume ratio, particularly in AC mode, which offered slower kinetics. At the same current intensity (4 A), increasing n from 1 to 3 caused the removal efficiency to increase from 27.3% to 51.6% in AC mode and from 92.5% to 99.4% in CA mode (Fig. 5(b)) and the energy consumption per order (E_{EO}) to decrease from 24.6 to 10.8 kW·h·m^{-3} in AC mode and from 3.0 to 1.5 kW·h·m^{-3} in CA mode (Fig. 5(c)). Moreover, the feasibility of the numbering-up strategy for scale-up was confirmed by the stable 2,4-DCP removal efficiency (Fig. S10 in Appendix A). Despite the similar cell voltages (4.7, 3.8, and 3.5 V for n = 1, 2, and 3, respectively) for the two modes, the energy consumption in CA mode was nearly one order of magnitude greater than that in AC mode because the decisive factor was effluent residual concentration (C_p; Eq. (2)) rather than the removal efficiency. The considerably higher energy consumption could be interpreted in the context of a higher C_p due to less efficient destruction of organic pollutants in AC mode. This corresponds to the lower current efficiency and COD removal in AC mode (68.7%–87.0% and 64.2%–87.9% lower, respectively) than those in CA mode (Fig. S11 in Appendix A). The lowest E_{EO} obtained at 1.5 kW·h·m^{-3} (99.4% removal) is in the range of values for the advanced electrochemical oxidation process of the membrane electrode on a laboratory scale (< 2.0 kW·h·m^{-3}) [20]. Compared with conventional electrochemical treatment (summarized in Table S3 in Appendix A), a higher energy consumption (several orders of kilowatt-hours per cubic meter) (Table S3 [37,38]) was the consequence of the higher thermodynamic potential necessary for ·OH production (2.38 V vs SHE) and side parasitic reactions, such as oxygen evolution by water electrolysis. Despite this, the TCE-based modularized process is still competitive for larger-scale decentralized treatment of high-salinity industrial wastewater.

Fig. 5. (a) Optical images of the modularized TCE electrolytic reactor (n = 1, 2, 3); (b) removal efficiency of 2,4-DCP and (c) energy consumption per order under AC and CA modes. Tests were performed at [2,4-DCP] of 10 mg·L^{-1}, total current of 4 A, and flow rate of 60 mL·min^{-1}.

4. Conclusions

Based on the above results, the following conclusions can be drawn. The TCE configuration with a titanium suboxide ceramic anode and stainless-steel cathode was shown to be suitable for scale-up of the reactor. In the TCE configuration, the electrode surface is orthogonal to electric field lines everywhere, and the ohmic resistance is inversely proportional to the length of the electrode. The TCE configuration can be operated in either AC or CA mode based on the flow direction, creating adjustable conditions for selective degradation of pollutants. In CA mode, 98% removal of 2,4-DCP and 72.5% removal of COD were achieved because the kinetic constant was one order of magnitude higher than that in AC mode under flow-through single-pass operation. The TCE configuration was also shown to be suitable for a numbering-up strategy to scale up the electrochemical reactor without increasing the ohmic resistance or reducing the specific electrode area, which achieved 99.4% removal of 2,4-DCP with an energy consumption of 1.5 kW·h·m^{-3} when three TCE modules were employed. This study provides a reasonable, easy-to-handle, and reliable strategy for scaling up REM reactors, which can also be extended to realize the removal of other recalcitrant organic pollutants and decentralized electrochemical wastewater treatment.

Compliance with ethics guidelines

Shuzhao Pei, Yi Wang, Shijie You, Zhanguo Li, and Nanqi Ren declare that they have no conflict of interest or financial conflicts to disclose.

Appendix A. Supplementary data

Supplementary data to this article can be found online at https://doi.org/10.1016/j.eng.2021.11.017.

References

[1] Moreira FC, Boaventura RAR, Brillas E, Vilar VJP. Electrochemical advanced oxidation processes: a review on their application to synthetic and real wastewaters. Appl Catal B 2017;202:217–61.
[2] Radjenovic J, Sedlak DL. Challenges and opportunities for electrochemical processes as next-generation technologies for the treatment of contaminated water. Environ Sci Technol 2015;49(19):11292–302.
[3] Zhu L, Santiago-Schübel B, Xiao H, Hollert H, Kueppers S. Electrochemical oxidation of fluoroquinolone antibiotics: mechanism, residual antibacterial activity and toxicity change. Water Res 2016;102:52–62.
[4] Guo L, Jing Y, Chaplin BP. Development and characterization of ultrafiltration TiO$_2$ Magnéli phase reactive electrochemical membranes. Environ Sci Technol 2016;50(3):1428–36.
[5] Lin H, Peng H, Feng X, Li X, Zhao J, Yang K, et al. Energy-efficient for advanced oxidation of bio-treated landfill leachate effluent by reactive electrochemical membranes (REMs): laboratory and pilot scale studies. Water Res 2021;190:116790.
[6] Zaky AM, Chaplin BP. Porous substoichiometric TiO$_2$ anodes as reactive electrochemical membranes for water treatment. Environ Sci Technol 2013;47 (12):6554–63.
[7] Ma J, Ma J, Zhang C, Song J, Dong W, Waite TD. Flow-electrode capacitive deionization (FCDI) scale-up using a membrane stack configuration. Water Res 2020;168:115186.
[8] Sun M, Wang X, Winter LR, Zhao Y, Ma W, Hedtke T, et al. Electrified membranes for water treatment applications. ACS EST Eng 2021;1(4):725–52.
[9] Noël T, Cao Y, Laudadio G. The fundamentals behind the use of flow reactors in electrochemistry. Acc Chem Res 2019;52(10):2858–69.
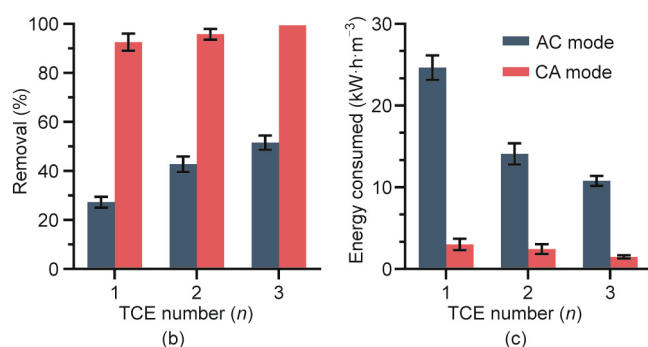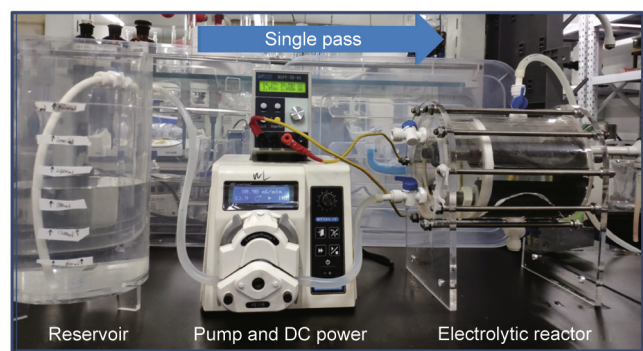
[10] Sulaymon AH, Abbar AH. Scale-up of electrochemical reactors. In: Kleperis J, Linkov V, editors. Electrolysis. London: IntechOpen Ltd.; 2012. p. 189–202.

[11] Goodridge F, Scott K. Electrochemical process engineering. New York: Springer Publishing Co.; 1995.

[12] Walsh F, Reade G. Design and performance of electrochemical reactors for efficient synthesis and environmental treatment. Part 2. Typical reactors and their performance. Analyst 1994;119(5):797–803.

[13] Walsh FC, Ponce de León C. Progress in electrochemical flow reactors for laboratory and pilot scale processing. Electrochim Acta 2018;280:121–48.

[14] Ni XY, Liu H, Wang C, Wang WL, Xu ZB, Chen Z, et al. Comparison of carbonized and graphitized carbon fiber electrodes under flow-through electrode system (FES) for high-efficiency bacterial inactivation. Water Res 2020;168:115150.

[15] Wang J, Zhi D, Zhou H, He X, Zhang D. Evaluating tetracycline degradation pathway and intermediate toxicity during the electrochemical oxidation over a Ti/Ti$_4$O$_7$ anode. Water Res 2018;137:324–34.

[16] Pourmahmoud N, Sadeghifar H, Torkavannejad A. A novel, state-of-the-art tubular architecture for polymer electrolyte membrane fuel cells: performance enhancement, size and cost reduction. Int J Heat Mass Transf 2017;108(Pt A):577–84.

[17] Rabuni MF, Li T, Punmeechao P, Li K. Electrode design for direct-methane micro-tubular solid oxide fuel cell (MT-SOFC). J Power Sources 2018;384:287–94.

[18] Ressel S, Laube A, Fischer S, Chica A, Flower T, Struckmann T. Performance of a vanadium redox flow battery with tubular cell design. J Power Sources 2017;355:199–205.

[19] You S, Liu B, Gao Y, Wang Y, Tang CY, Huang Y, et al. Monolithic porous Magnéli-phase Ti$_4$O$_7$ for electro-oxidation treatment of industrial wastewater. Electrochim Acta 2016;214:326–35.

[20] Gayen P, Chen C, Abiade JT, Chaplin BP. Electrochemical oxidation of atrazine and clothianidin on Bi-doped SnO$_2$–TinO$_{2n-1}$ electrocatalytic reactive electrochemical membranes. Environ Sci Technol 2018;52(21):12675–84.

[21] Pei S, You S, Ma J, Chen X, Ren N. Electron spin resonance evidence for electro-generated hydroxyl radicals. Environ Sci Technol 2020;54(20):13333–43.

[22] Corović S, Pavlin M, Miklavčič D. Analytical and numerical quantification and comparison of the local electric field in the tissue for different electrode configurations. Biomed Eng Online 2007;6:37.

[23] Hankin A, Bedoya-Lora FE, Ong CK, Alexander JC, Petter F, Kelsall GH. From millimetres to metres: the critical role of current density distributions in photo-electrochemical reactor design. Energy Environ Sci 2017;10:346–60.

[24] Zhou J, Wang T, Xie X. Rationally designed tubular coaxial-electrode copper ionization cells (CECICs) harnessing non-uniform electric field for efficient water disinfection. Environ Int 2019;128:30–6.

[25] Zhou J, Wang T, Xie X. Locally enhanced electric field treatment (LEEFT) promotes the performance of ozonation for bacterial inactivation by disrupting cell membrane. Environ Sci Technol 2020;54(21):14017–25.

[26] Sun L, Wang X, Li M, Zhang S, Wang Q. Anodic titania nanotubes grown on titanium tubular electrodes. Langmuir 2014;30(10):2835–41.

[27] Perry SC, Ponce de León C, Walsh FC. Review—the design, performance and continuing development of electrochemical reactors for clean electrosynthesis. J Electrochem Soc 2020;167(15):155525.

[28] Ahn Y, Hatzell MC, Zhang F, Logan BE. Different electrode configurations to optimize performance of multi-electrode microbial fuel cells for generating power or treating domestic wastewater. J Power Sources 2014;249:440–5.

[29] Jaramillo-Gutiérrez MI, Carreño-Lizcano MI, Ruiz-Lizarazo JO, Pedraza-Avella JA, Rivero EP, Cruz-Díaz MR. Design, mathematical modelling, and numerical simulation of a novel tubular photoelectrochemical reactor and experimental validation by residence time distribution and mass transfer coefficients. Chem Eng J 2020;386:123895.

[30] Lei Y, Zhan Z, Saakes M, van der Weijden RD, Buisman CJN. Electrochemical recovery of phosphorus from wastewater using tubular stainless-steel cathode for a scalable long-term operation. Water Res 2021;199:117199.

[31] Wang AJ, Wang HC, Cheng HY, Liang B, Liu WZ, Han JL, et al. Electrochemistry-stimulated environmental bioremediation: development of applicable modular electrode and system scale-up. Environ Sci Ecotech 2020;3:100050.

[32] Wang G, Liu Y, Ye J, Lin Z, Yang X. Electrochemical oxidation of methyl orange by a Magnéli phase Ti$_4$O$_7$ anode. Chemosphere 2020;241:125084.

[33] Deborde M, von Gunten U. Reactions of chlorine with inorganic and organic compounds during water treatment—kinetics and mechanisms: a critical review. Water Res 2008;42(1–2):13–51.

[34] Cheng X, Guo H, Li W, Yang B, Wang J, Zhang Y, et al. Metal-free carbocatalysis for persulfate activation toward nonradical oxidation: enhanced singlet oxygen generation based on active sites and electronic property. Chem Eng J 2020;396:125107.

[35] Ma Y, Gu Y, Jiang D, Mao X, Wang D. Degradation of 2,4-DCP using persulfate and iron/E-carbon micro-electrolysis coupling system. J Hazard Mater 2021;413:125381.

[36] Guo H, Kim Y. Scalable multi-electrode microbial electrolysis cells for high electric current and rapid organic removal. J Power Sources 2018;391:67–72.

[37] Martínez-Huitle CA, Rodrigo MA, Sirés I, Scialdone O. Single and coupled electrochemical processes and reactors for the abatement of organic water pollutants: a critical review. Chem Rev 2015;115(24):13362–407.

[38] He W, Dong Y, Li C, Han X, Liu G, Liu J, et al. Field tests of cubic-meter scale microbial electrochemical system in a municipal wastewater treatment plant. Water Res 2019;155:372–80.